Supplementary Information for

Micro-structured P-N junction surface: large-scale preparation, antifouling properties, and synergistic antibacterial mechanism

Mengfei Ni[a,†], Wenwen Li[a,b,†], Bing Yuan[b,*], Shuai Zou[a], Wei Cheng[a], Kai Yang[a], Jiandong Su[c,*], Bingwei Sun[c], Xiaodong Su[a,*]

[a] School of Physical Science and Technology, and Jiangsu Key Laboratory of Thin Films, Soochow University, Suzhou 215006, China

[b] Songshan Lake Materials Laboratory, Dongguan 523808, China

[c] Suzhou Municipal Hospital, Suzhou 215008, China

[†]These authors contributed equally to this work.

*Corresponding authors. yuanbing@sslab.org.cn (B.Y.); jiandongsu@njmu.edu.cn (J.S.); xdsu@suda.edu.cn (X.S.)

Experimental details; supplementary images (Figure S1-S7) and tables (Table S1, S2).

Experimental Section

Sample preparation: Commercial gallium-doped p-type and phosphorus-doped n-type silicon wafers were used in this work. The wafers were (100) oriented, had a specific resistivity of 1~3 Ω·cm and a thickness of 170±10 μm. The mature alkaline texturing technology of monocrystalline silicon solar cells was used for the preparation of silicon wafers with micro-pyramid surfaces [1, 2]. After that, p-n junctions were fabricated through boron (B) doping of n-type wafers (abbreviated as p^+n-Si) and phosphorus (P) doping of p-type wafers (termed as n^+p-Si) [3, 4].

Characterization of the micro-pyramid topography: The surface topography of the substrates were characterized using a scanning electron microscope (SEM, HITACHI S-4700) and an atomic force microscope (AFM, MFP-3D, Oxford Instruments, USA). Distributions of the pyramid parameters, including base size, height, tip angle, and inter-tip distance, were analyzed based on at least three SEM images using the Nano-Measurer 1.2 software.

Bacterial Strains: Three standard stains were used, i.e., *Escherichia coli* ATCC 25922, *Pseudomonas aeruginosa* ATCC 27853, and *Staphylococcus aureus* ATCC 25923 (ATCC, Manassas, VA, USA). The fungus, *Candida albicans*, was obtained by clinical isolation.

Live/Dead staining assay: The *E. coli* was grown to the midlogarithmic phase at 37 ℃. The optical density of the bacterial solution was adjusted to $OD_{600\ nm} = 0.1$. The substrates (i.e., bare glass, polished *p*-Si, *p*-Si, n^+p-Si, and p^+n-Si) were immersed in 1 mL of bacterial fluid and incubated for 0.5 h, in the dark or under light illumination (by a 300 W xenon arc lamp with an ultraviolet cut-off filter). The bare glass was used as a control. After incubation, the substrates were washed three times with phosphate buffer saline (PBS) and stained successively with DAPI and PI. The substrates were then observed under an inverted confocal microscope (LSM 710, Zeiss) equipped with a 63× oiled objective lens. All images were captured under the same instrumental settings. Quantitative analysis of the fluorescence images was performed using ImageJ. The bacterial survival rate on each substrate was obtained following

$$\text{Survival rate (\%)} = \left(1 - \frac{N_{\text{red fluorescence}}}{N_{\text{blue fluorescence}}}\right) \times 100\%$$. At least three independent experiments were performed for each condition.

SEM characterization of bacteria: SEM was used to characterize the morphology of bacteria on different substrate surfaces. The *E. coli* was grown to the midlogarithmic phase and incubated with different substrates for 4 hours, in the dark or under light illumination. After that, the bacteria were fixed with 4% glutaraldehyde for at least 10 h, dehydrated with a series of ethanol solutions (30%, 50%, 70%, 90%, 95% and 100 %), and lyophilized. SEM (HITACHI S-4700) images were acquired after gold coating.

Bacterial membrane permeability test: To test the permeability of bacterial membranes upon exposure to different substrates, quantitative determination of the leakage contents (e.g., nucleic acid and protein) from the bacteria to the environment was performed following previous protocols [5]. Briefly, 2 mL of *E. coli* solution, with an optical density value at 600 nm of 1.2 (OD_{600} = 1.2), was exposed to different substrates and incubated for 4 h, in the dark or under light illumination. The solution was then centrifuged at 8000 rpm for 10 min, and the supernatant was collected for analysis. The protein concentration was determined directly, following the Enhanced BCA Protein Assay Kit protocol (cat# P0010; Beyotime, Jiangsu, China). The nucleic acid concentration was obtained based on the OD_{260} value of the supernatant, after being filtered through 0.22 μm pores [6]. All experimental results were from at least three independent tests.

Detection of ROS production: The amount of ROS produced in different conditions was determined using a Reactive Oxygen Species Assay Kit. The fluorescence-free 2′,7′-dichlorofluorescein diacetate (DCFH-DA) can be converted into fluorescent 2′,7′-dichlorofluorescein (DCF) by reaction with ROS, which can be detected by a microplate reader (Thermo Scientific, Varioskan LUX) [7]. Briefly, 2 mL of *E. coli* solution was exposed to different substrates and incubated for 30 min, in the dark or under light illumination (with a 25 W incandescent lamp). The ROS content was determined following the ROS Assay Kit protocol (H131224, Aladdin). All experimental results were from at least three independent tests.

Optical and electrical tests of the micro-pyramid substrate with p-n junction: The ultraviolet-visible diffuse reflection spectroscopy test (UV-vis DRS) was performed using a UV-VIS-NIR spectrometer (UV-3600, Shimadzu, Japan). The photoluminescence imaging (PLI) experiment was performed using a PL testing equipment (PL, LIS-R3). This technique is generally used to analyze the spatial variations of photogenerated electrons in a silicon wafer. The current density-voltage (*J-V*) curves were obtained using a programmable Keithley 2400 source meter at 100 $mW \cdot cm^{-2}$ under AM 1.5 G solar irradiation (SAN-EI, Class AAA solar simulator, XES-70S1).

Test settlement in ICU: Samples (i.e., bare glass, polished Si, p^+n-Si and n^+p-Si) with a large size of 10 cm × 10 cm were placed near the window in an ICU ward. Thus, the samples were exposed to sunlight during the day and indoor light in the night. After being kept for two weeks (May 1-14，2021; May 15-29, 2021; June 1-14, 2021), the samples were collected for analysis. Part of the samples was processed for SEM observation. The other part was used for bacterial collection. Briefly, the bacteria were further incubated in culture dishes for 48 hours. Then, the colonies were identified and counted by Automatic Rapid Biomass Spectrum Detection system (Bruker Microflex LT/SH), which is based on Matrix-assisted laser desorption / ionization time of flight (MALDI-TOF) mass spectrometric analysis [8]. The laser excites the bacteria and matrix on the target plate, and leave the bacterial protein in the vacuum flight tube. By detecting the difference of protein flight time, the detector establishes a curve map and compares it with the information in the database, to determine the possible bacterial species [9].

Bacterial smear: To simulate the real "contact" conditions between bacteria and surfaces, typical standard strains, including the *S. aureus*, *P. aeruginosa, E. coli* and *C. albicans*, which are mainly spread by contact, were detected by smear and cultivation. Briefly, the standard strains were diluted to 1.5×10^8 CFU per mL with normal saline and smeared on the surface of large-size samples by cotton swabs that have been clinically sterilized, and incubated under ambient illumination for 6 h. The bacteria on the samples were collected and further incubated in culture dishes for 48 hours before

colony counting.

Data Statistics: All data were presented as means with standard deviations (SD). The significance analysis between two groups was tested using the Two-sample t-Test of OriginPro (Origin Lab Corporation, Northampton, MA, USA.).

Supplementary images

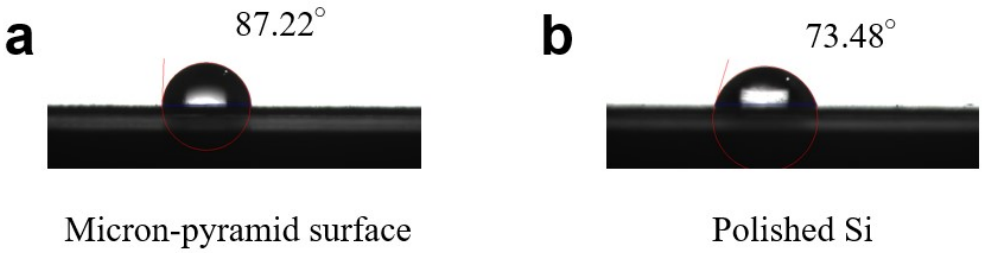

Figure S1. Water contact angle tests of different surfaces, including the micron-pyramid *n*-Si surface (a) and the polished *n*-Si (b).

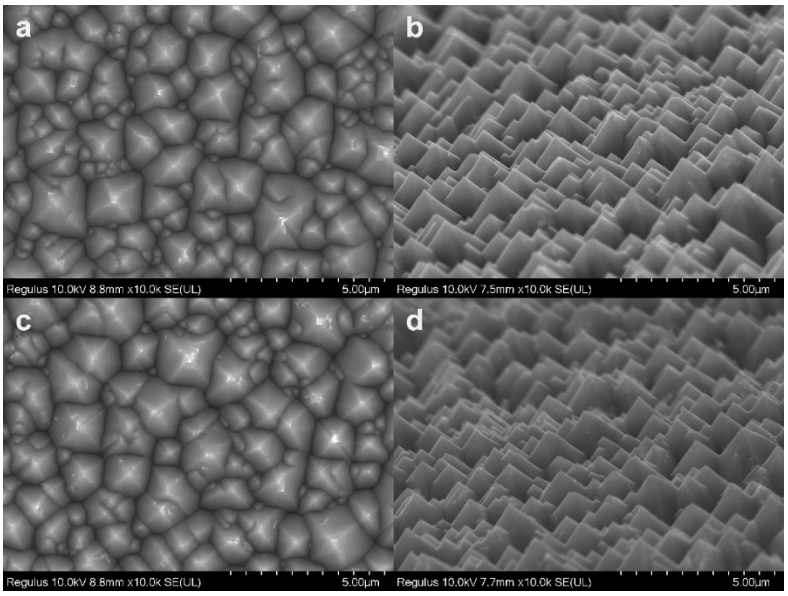

Figure S2. Scanning electron microscopy (SEM) images of the micron-pyramid surface before and after element diffusion. (a, b) Top and side view of the surface before element diffusion. (c, d) After element diffusion.

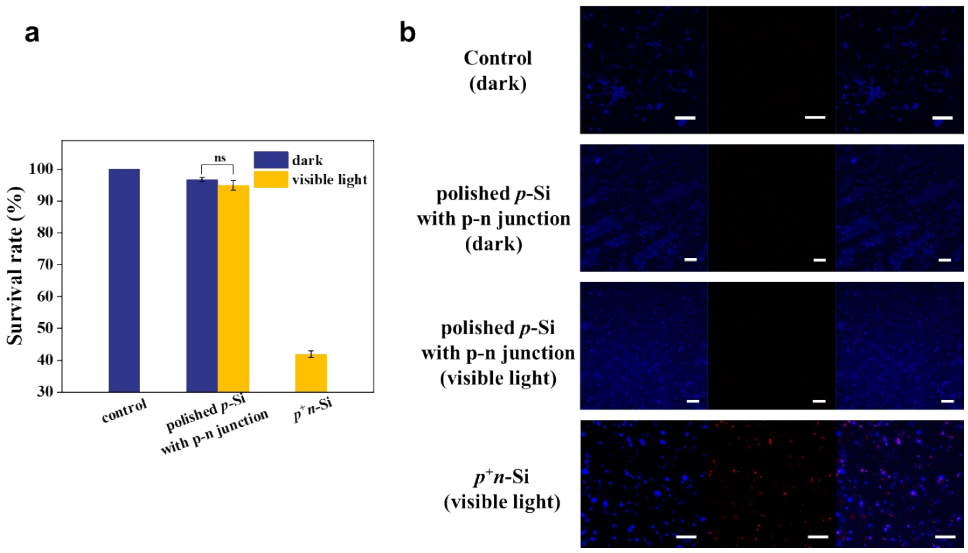

Figure S3. Antibacterial performance of different surfaces. *E. coli* bacteria were incubated with the substrates in the dark or under visible light illumination for 0.5 h before DAPI and PI staining. (a) Histograms showing survival rate of bacteria in different conditions. Data show normalized mean and standard error of at least three independent experiments. (b) Representative confocal micrographs acquired in the DAPI, PI and overlaid channels. Scale bar refers to 10 μm.

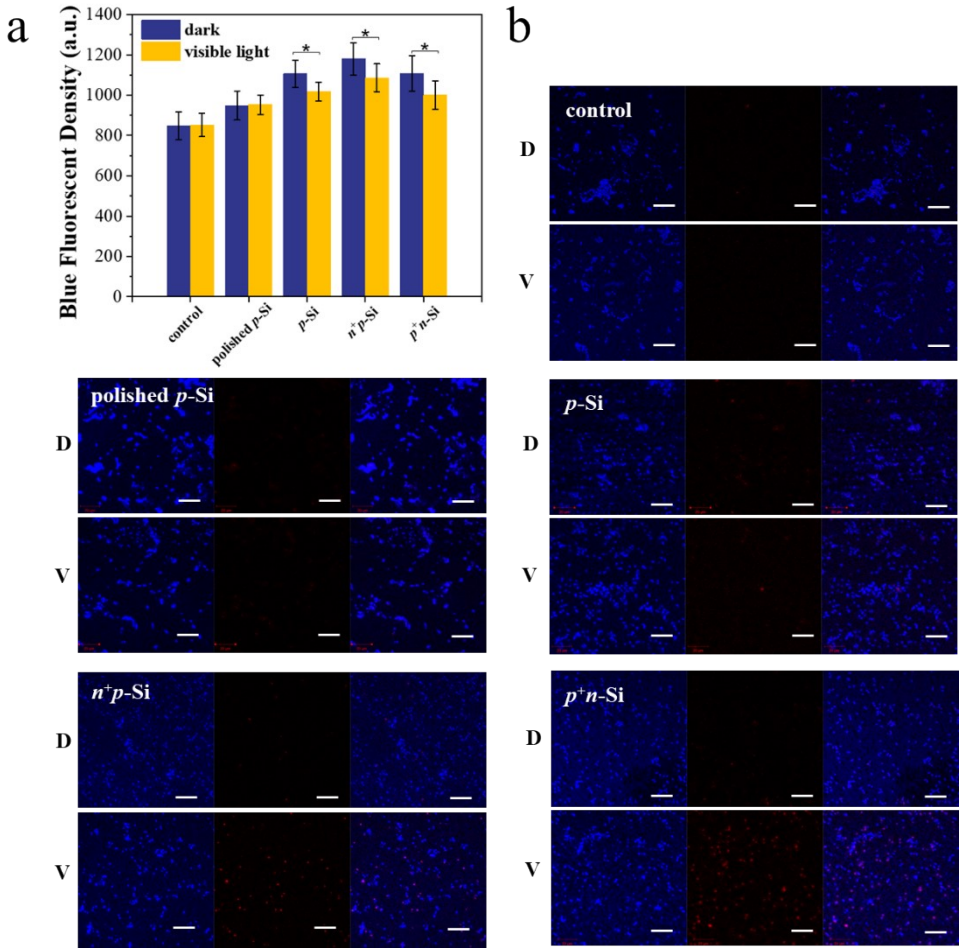

Figure S4. Comparison of blue fluorescent density on different surfaces. (a) Histograms showing the blue fluorescent density on different surfaces in different illumination conditions. Data show normalized mean and standard error of at least three independent experiments. (b) Representative confocal micrographs acquired in the DAPI, PI and overlaid channels. 'D' and 'V' refer to "dark" and "visible light", respectively. Scale bar refers to 10 μm.

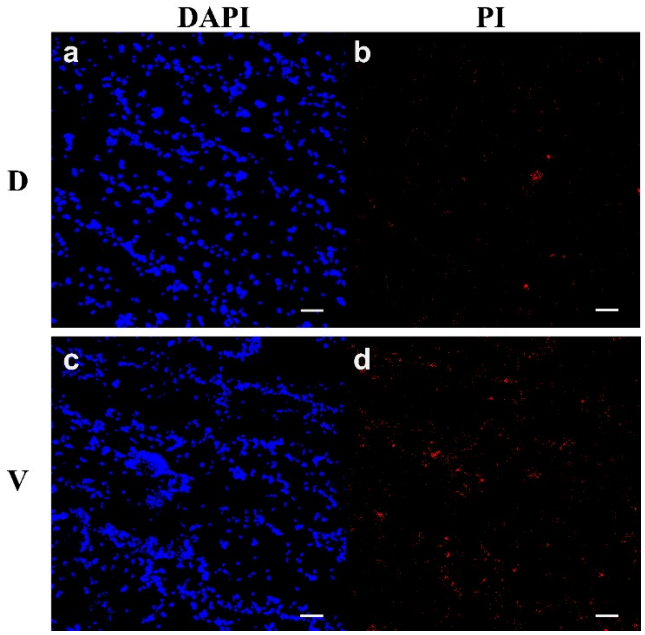

Figure S5. Representative confocal micrographs of the *Staphylococcus aureus* exposed surfaces of the boron-doped *n*-type micron-pyramid silicon wafer (termed as $p^{+}n$-Si). The bacteria were incubated in the dark ('D') or under light illumination ('V') for 0.5 h before DAPI and PI staining. Scale bar refers to 10 μm. The images were obtained in the DAPI (left) and PI (right) channels.

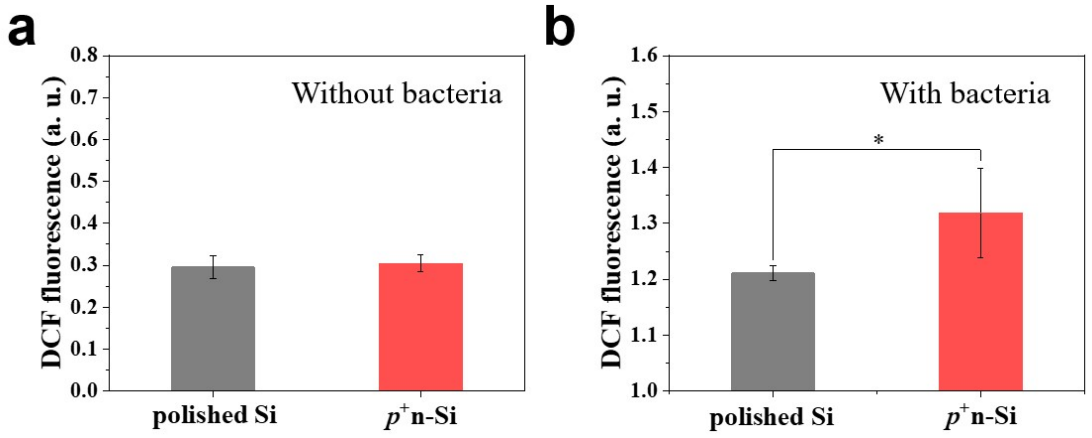

Figure S6. DCF fluorescence determination on different surfaces without or with bacteria. The fluorescent intensity refers to ROS content.

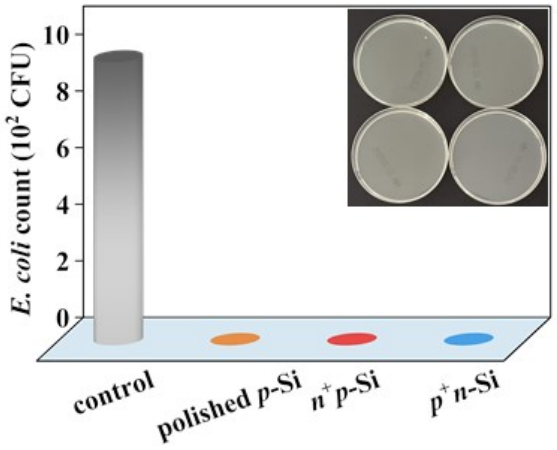

Figure S7. Antibacterial performance of different surfaces against *E. coli*. Digital photos of the culture dishes, with a diameter of 6 cm, showing bacteria collected from different sample surfaces are shown as insets. Data show normalized mean and standard error of three independent experiments.

Corresponding note

Almost no *E. coli* is observed especially for the silicon cases, probably due to the low tolerance of *E. coli* to dry aerobic environment [10].

Supplementary tables

Table S1. Specie identification and brief introduction of the bacteria collected on the substrates exposed in an ICU for two weeks. The bacterial specie was determined by mass spectrometry.

Classification	Species	Distribution	Pathogenicity	Ref
Gram-negative	*E. coli*	Fecal-oral route of transmission, etc.	Local tissue and organ infections, such as the gastrointestinal tract, etc.	[11]
Gram-positive	*Bacillus cereus*	water, air, etc.	Gastroenteritis and vomiting, etc.	[12, 13]
	Kocuria rosea	Skin, respiratory tract, soil, water, etc.	Pneumonia or catheter infection in immunodeficiency patients, etc.	[14, 15]
	Micrococcus luteus	Water, skin surface, etc.	Catheter infection in immunodeficiency patients, etc.	[16, 17]
	Staphylococcus hominis	Skin, intestines, etc.	Nosocomial cross infection, etc.	[18, 19]
Fungus	*Alternaria alternata*	Air, soil, etc.	Allergic airways disease, etc.	[20]
	Aspergillus fumigatus	Lungs, soil, decaying organic matter, etc.	Organ infections in immunodeficiency patients, etc.	[21, 22]

Corresponding note

The results of Matrix-assisted laser desorption / ionization time of flight (MALDI-TOF) mass spectrometer analysis show that the bacteria are mainly composed of Rhizobium

radiobacter, Kocuria rosea, Bacillus cereus, Micrococcus luteus and Alternaria alternata (as detailed in Table S1). According to the classification of Gram staining, these bacteria can be classified into Gram-negative and Gram-positive bacteria, respectively. In addition, A. alternata belongs to fungi. Counting statistics according to categories, the survival status of bacteria on different surfaces is obtained (as shown in Figure 5c).

Table S2. Brief introduction of the bacteria used in the contact infection test.

Species	Classification	Distribution	Pathogenicity	Ref
S. aureus	Gram-positive	Skin, nose, throat, sewage, etc.	Bacteremia, endocarditis, skin infections, etc.	[23, 24]
P. aeruginosa	Gram-negative	Skin, water, respiratory tract, intestine, etc.	Fatal infections in immunocompromised individuals, etc.	[25, 26]
C. albicans	Fungus	Skin, medical equipment, clothing, etc.	Life-threatening systemic fungal infections, etc.	[27, 28]

Corresponding note

Standard strains of *S. aureus*, *P. aeruginosa*, *E. coli* and *Candida albicans* were representatively used as Gram-positive bacteria, Gram-negative bacteria, and fungus, respectively. The brief introduction on distribution and pathogenicity of these bacteria are summarized in **Table S2**.

References

[1] Y. Li, S. Zhong, Y. Zhuang, L. Yang, F. Meng, W. Wang, Z. Li, W. Shen, Quasi-omnidirectional ultrathin silicon solar cells realized by industrially compatible processes, Adv. Electron. Mater. 5(3) (2019) 1800858.

[2] S. Zhong, W. Wang, Y. Zhuang, Z. Huang, W. Shen, All-solution-processed random Si nanopyramids for excellent light trapping in ultrathin solar cells, Adv. Funct. Mater. 26(26) (2016) 4768-4777.

[3] A.Z. H. Ghembaza, R. Saïm, M. Pasquinelli., Optimization of phosphorus emitter formation from $POCl_3$ diffusion for p-Type silicon solar cells processing, Silicon 10(2) (2018) 377-386.

[4] J. Armand, C. Oliver, F. Martinez, B. Semmache, M. Gauthier, A. Foucaran, Y. Cuminal, Modeling of the boron emitter formation process from BCl_3 diffusion for N-type silicon solar cells processing., Adv Mat Res 324 (2011) 261-264.
[5] J. Li, L. Tan, X. Liu, Z. Cui, X. Yang, K.W.K. Yeung, P.K. Chu, S. Wu, Balancing bacteria-osteoblast competition through selective physical puncture and biofunctionalization of ZnO/polydopamine/arginine-glycine-aspartic acid-cysteine nanorods, ACS Nano 11(11) (2017) 11250-11263.
[6] S. Liang, Q. Dang, C. Liu, Y. Zhang, Y. Wang, W. Zhu, G. Chang, H. Sun, D. Cha, B. Fan, Characterization and antibacterial mechanism of poly(aminoethyl) modified chitin synthesized via a facile one-step pathway, Carbohydr Polym 195 (2018) 275-287.
[7] J. Li, Z. Li, X. Liu, C. Li, Y. Zheng, K.W.K. Yeung, Z. Cui, Y. Liang, S. Zhu, W. Hu, Y. Qi, T. Zhang, X. Wang, S. Wu, Interfacial engineering of $Bi_2S_3/Ti_3C_2T_x$ MXene based on work function for rapid photo-excited bacteria-killing, Nat Commun 12(1) (2021) 1224.
[8] D. Dupont, A.C. Normand, F. Persat, M. Hendrickx, R. Piarroux, M. Wallon, Comparison of matrix-assisted laser desorption ionization time of flight mass spectrometry (MALDI-TOF MS) systems for the identification of moulds in the routine microbiology laboratory, Clin Microbiol Infect 25(7) (2019) 892-897.
[9] R. Patel, Matrix-assisted laser desorption ionization-time of flight mass spectrometry in clinical microbiology, Clin Infect Dis 57(4) (2013) 564-72.
[10] Y. Fang, L.M. McMullen, M.G. Ganzle, Effect of drying on oxidation of membrane lipids and expression of genes encoded by the Shiga toxin prophage in Escherichia coli, Food Microbiol. 86 (2020) 103332.
[11] J. Vila, E. Saez-Lopez, J.R. Johnson, U. Romling, U. Dobrindt, R. Canton, C.G. Giske, T. Naas, A. Carattoli, M. Martinez-Medina, J. Bosch, P. Retamar, J. Rodriguez-Bano, F. Baquero, S.M. Soto, Escherichia coli: an old friend with new tidings, FEMS Microbiol. Rev. 40(4) (2016) 437-463.
[12] D. Enosi Tuipulotu, A. Mathur, C. Ngo, S.M. Man, Bacillus cereus: epidemiology, virulence factors, and host-pathogen interactions, Trends Microbiol. 29(5) (2021) 458-471.
[13] D. Fox, A. Mathur, Y. Xue, Y. Liu, W.H. Tan, S. Feng, A. Pandey, C. Ngo, J.A. Hayward, Atmosukarto, II, J.D. Price, M.D. Johnson, N. Jessberger, A.A.B. Robertson, G. Burgio, D.C. Tscharke, E.M. Fox, D.L. Leyton, N.O. Kaakoush, E. Martlbauer, S.H. Leppla, S.M. Man, Bacillus cereus non-haemolytic enterotoxin activates the NLRP3 inflammasome, Nat Commun 11(1) (2020) 760.
[14] N. Mori, Y. Nishihara, H. Tayama, A. Higuchi, Y. Aoki, Peripherally inserted central catheter-related bloodstream infection caused by Kocuria marina in an elderly man, INFECTION 45(5) (2017) 683-686.
[15] C.C. Lai, J.Y. Wang, S.H. Lin, C.K. Tan, C.Y. Wang, C.H. Liao, C.H. Chou, Y.T. Huang, H.I. Lin, P.R. Hsueh, Catheter-related bacteraemia and infective endocarditis caused by Kocuria species, Clin Microbiol Infect 17(2) (2011) 190-2.
[16] V. Celiksoy, R.L. Moses, A.J. Sloan, R. Moseley, C.M. Heard, Synergistic in vitro antimicrobial activity of pomegranate rind extract and Zinc (II) against Micrococcus luteus under planktonic and biofilm conditions, Pharmaceutics 13(6) (2021) 851.
[17] S.S. Benedict M. Selladurai, Subramania Aiyar &Abdul R. Mohamad, Intracranial suppuration caused by Micrococcus luteus, BRITISH JOURNAL OF NEUROSURGERY 7(2) (1993) 205-207.
[18] O.C. Smibert, H.L. Wilson, A. Sohail, S. Narayanasamy, M.B. Schultz, S.A. Ballard, J.C. Kwong, J. de Boer, C.O. Morrissey, A.Y. Peleg, G.I. Snell, M.A. Paraskeva, A.W.J. Jenney, Donor-derived

Mycoplasma hominis and an apparent cluster of M. hominis cases in solid organ transplant recipients, Clin Infect Dis 65(9) (2017) 1504-1508.
[19] F. Chaves, M. Garcia-Alvarez, F. Sanz, C. Alba, J.R. Otero, Nosocomial spread of a Staphylococcus hominis subsp. novobiosepticus strain causing sepsis in a neonatal intensive care unit, J. Clin. Microbiol. 43(9) (2005) 4877-4879.
[20] M.F. Gabriel, I. Postigo, C.T. Tomaz, J. Martinez, Alternaria alternata allergens: Markers of exposure, phylogeny and risk of fungi-induced respiratory allergy, Environ Int 89-90 (2016) 71-80.
[21] A. Arastehfar, A. Carvalho, J. Houbraken, L. Lombardi, R. Garcia-Rubio, J.D. Jenks, O. Rivero-Menendez, R. Aljohani, I.D. Jacobsen, J. Berman, N. Osherov, M.T. Hedayati, M. Ilkit, D. Armstrong-James, T. Gabaldon, J. Meletiadis, M. Kostrzewa, W. Pan, C. Lass-Florl, D.S. Perlin, M. Hoenigl, Aspergillus fumigatus and aspergillosis: From basics to clinics, Stud. Mycol. 100 (2021) 100115.
[22] J.P. Latge, G. Chamilos, Aspergillus fumigatus and Aspergillosis in 2019, Clin. Microbiol. Rev. 33(1) (2019) e00140-18.
[23] N.A. Turner, B.K. Sharma-Kuinkel, S.A. Maskarinec, E.M. Eichenberger, P.P. Shah, M. Carugati, T.L. Holland, V.G. Fowler, Jr., Methicillin-resistant Staphylococcus aureus: an overview of basic and clinical research, Nat. Rev. Microbiol. 17(4) (2019) 203-218.
[24] A.S. Lee, H. de Lencastre, J. Garau, J. Kluytmans, S. Malhotra-Kumar, A. Peschel, S. Harbarth, Methicillin-resistant Staphylococcus aureus, Nat. Rev. Dis. Primers 4 (2018) 18033.
[25] M.D.M. Cendra, E. Torrents, Pseudomonas aeruginosa biofilms and their partners in crime, Biotechnol. Adv. 49 (2021) 107734.
[26] M.T.T. Thi, D. Wibowo, B.H.A. Rehm, Pseudomonas aeruginosa biofilms, Int. J. Mol. Sci. 21(22) (2020) 8671.
[27] Y. Lee, E. Puumala, N. Robbins, L.E. Cowen, Antifungal drug resistance: molecular mechanisms in Candida albicans and beyond, Chem. Rev. 121(6) (2021) 3390-3411.
[28] S.W. Kashem, D.H. Kaplan, Skin Immunity to Candida albicans, Trends Immunol. 37(7) (2016) 440-450.